# Characterization of a novel fusion gene EML4-NTRK3 in a case of recurrent congenital fibrosarcoma

COLD SPRING HARBOR
Molecular Case Studies

RESEARCH ARTICLE

# Characterization of a novel fusion gene *EML4-NTRK3* in a case of recurrent congenital fibrosarcoma

Sarah Tannenbaum-Dvir,[1] Julia L. Glade Bender,[1] Alanna J. Church,[2] Katherine A. Janeway,[3] Marian H. Harris,[2] Mahesh M. Mansukhani,[4] Peter L. Nagy,[4] Stuart J. Andrews,[4] Vundavalli V. Murty,[4] Angela Kadenhe-Chiweshe,[5] Eileen P. Connolly,[6] Andrew L. Kung,[1] and Filemon S. Dela Cruz[1]

[1]Columbia University Medical Center, Department of Pediatric Oncology/Hematology/Stem Cell Transplantation, Department of Pediatrics, New York, New York 10032, USA; [2]Harvard Medical School, Department of Pathology, Boston, Massachusetts 02115, USA; [3]Harvard Medical School, Department of Pediatric Oncology/Hematology, Boston, Massachusetts 02115, USA; [4]Columbia University Medical Center, Department of Pathology and Cell Biology, New York, New York 10032, USA; [5]Columbia University Medical Center, Department of Surgery, New York, New York 10032, USA; [6]Columbia University Medical Center, Department of Radiation Oncology, New York, New York 10032, USA

**Abstract** We describe the clinical course of a recurrent case of congenital fibrosarcoma diagnosed in a 9-mo-old boy with a history of hemimelia. Following complete surgical resection of the primary tumor, the patient subsequently presented with bulky bilateral pulmonary metastases 6 mo following surgery. Molecular characterization of the tumor revealed the absence of the prototypical *ETV6-NTRK3* translocation. However, tumor characterization incorporating cytogenetic, array comparative genomic hybridization, and RNA sequencing analyses, revealed a somatic t(2;15)(2p21;15q25) translocation resulting in the novel fusion of *EML4* with *NTRK3*. Cloning and expression of *EML4-NTRK3* in murine fibroblast NIH 3T3 cells revealed a potent tumorigenic phenotype as assessed in vitro and in vivo. These results demonstrate that multiple fusion partners targeting *NTRK3* can contribute to the development of congenital fibrosarcoma.

Corresponding authors: fd2177@cumc.columbia.edu, akung@columbia.edu



**Ontology terms:** congenital fibrosarcoma, abnormality of the musculature of the limbs

Published by Cold Spring Harbor Laboratory Press

doi: 10.1101/mcs.a000471

## INTRODUCTION

Congenital fibrosarcoma is a soft tissue sarcoma that presents in children under the age of 1 yr and represents 5%–10% of sarcomas in this age group (Orbach et al. 2010). Complete surgical resection of the primary tumor is the primary mode of treatment for congenital fibrosarcoma and results in overall survival rates of >90% (Orbach et al. 2010). Metastatic disease has been described for cases of congenital fibrosarcoma but occurs rarely (Bourgeois et al. 2000). In contrast to adult fibrosarcoma, use of systemic chemotherapy in neoadjuvant and adjuvant settings is effective in controlling and curing disease (Orbach et al. 2010).

Diagnosis of congenital fibrosarcoma is made based on histologic appearance, consisting of short spindle cells arranged in a fascicular growth pattern (herringbone pattern) (Gupta et al. 2004). Congenital fibrosarcoma classically has positive staining for vimentin but is negative for other lineage markers (pancytokeratin, EMA, desmin, HHF35, SMA, myogenin, MYOD1, CD34, and S100 protein). A majority of congenital fibrosarcoma cases

are characterized by the *ETV6-NTRK3* translocation (Knezevich et al. 1998b; Bourgeois et al. 2000), which has also been described in other neoplastic diseases such as mesoblastic nephroma (Rubin et al. 1998; Knezevich et al. 1998a) and secretory breast carcinoma (Tognon et al. 2002). Fluorescence in situ hybridization (FISH) using break-apart probes to detect a translocation of the *ETV6* and/or *NTRK3* genes is routinely used to confirm diagnosis of congenital fibrosarcoma (Bourgeois et al. 2000). We describe a case of congenital fibrosarcoma harboring a novel chromosomal translocation of *NTRK3*.

## RESULTS

### Clinical Presentation and Family History

A 9-mo-old male patient with a history of left upper extremity hemimelia presented with a left distal radial lytic soft tissue mass (Fig. 1A,B). The child was the result of an uncomplicated pregnancy, and aside from the hemimelia, there were no other congenital anomalies. There was no history of significant prenatal exposures, and the family history was unremarkable.

Biopsy of the soft tissue mass suggested a diagnosis of congenital fibrosarcoma based on histologic appearance (Fig. 1F) and positive staining for vimentin alone. The index case exhibited a high mitotic index with up to 50 mitoses per 10 high power fields (Fig. 1H). Cytogenetic analysis of the biopsied tumor revealed a complex karyotype consisting of chromosomal gains and a translocation localized to t(2;15)(p21;q24) (Fig. 1C). However, FISH analysis using an *ETV6* break-apart probe showed no evidence of rearrangement (Fig. 1D) indicating the absence of the characteristic *ETV6-NTRK3* fusion gene associated with congenital fibrosarcoma (Knezevich et al. 1998b).

The patient underwent a surgical amputation resulting in a complete resection of the tumor with negative margins. Postoperative surveillance imaging 6 mo after resection revealed multiple bilateral lung metastases (Fig. 1E). Three days after imaging, the patient clinically decompensated and was admitted to the Pediatric Intensive Care Unit where a biopsy of his pulmonary lesions confirmed a diagnosis of relapsed congenital fibrosarcoma with histologic features identical to his initial presentation (Fig. 1F).

The patient was treated as per the Children's Oncology Group (COG) protocol ARST0332 (NCT00346164) consisting of several cycles of ifosfamide and doxorubicin. In addition, he received targeted radiation therapy to his right lung metastasis to a total dose of 5000 cGy. All sites of disease responded to therapy as assessed by computed tomography (CT) imaging, but positron emission tomography (PET)-CT imaging revealed mild residual avidity in his left lung lesions. The patient underwent complete resection of the left-sided PET avid lesions, which revealed small foci of viable tumor (Fig. 1G). Given the presence of residual tumor, the patient received further systemic chemotherapy consisting of four cycles of topotecan and cyclophosphamide (Saylors et al. 1998). Upon completion of systemic chemotherapy, the patient underwent surgical resection of his residual right-sided lesions, which revealed no evidence of viable tumor. The patient is clinically well and remains free of disease more than 1 yr after completion of therapy.

### Genomic Analyses

Because of the patient's uncharacteristically aggressive clinical course and in the absence of the prototypical *ETV6-NTRK3* translocation, the histological diagnosis of congenital fibrosarcoma was in question. To more comprehensively characterize the molecular basis of disease, the patient was enrolled onto a multicenter targeted gene sequencing research study

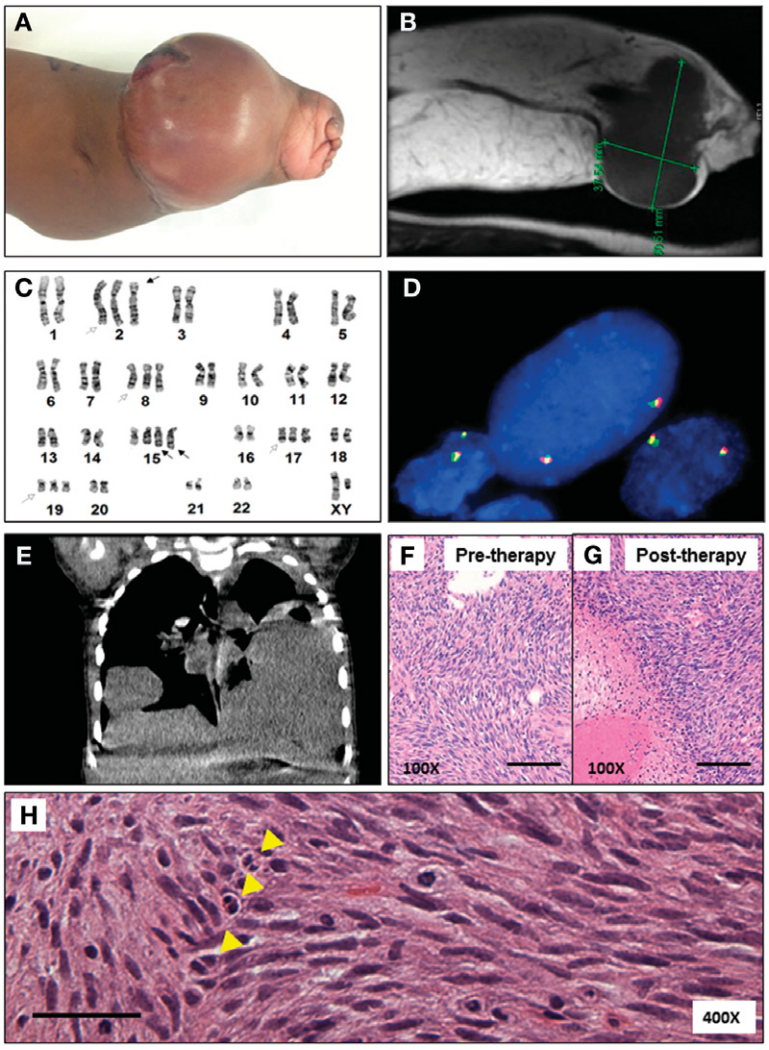


**Figure 1.** (*A*) Image of patient with left upper extremity hemimelia and distal arm soft tissue mass. (*B*) MRI imaging further demonstrates a 3.7 × 6 × 4.9-cm soft tissue mass within the distal left forearm. (*C*) Karyotype derived from tissue of the initial forearm lesion shows a complex karyotype: 52, XY, +2 t(2;15)(p21;q24), +8, +15, +der(15)t(2;15)(p21;q24), +17, +19, −1D. White arrows indicate gains in Chromosomes 2, 8, 17, and 19. Black arrows show a balanced t(2;15)(p21;q24) translocation as well as an extra copy of der(15)t(2;15). (*D*) Dual-colored FISH using *ETV6* break-apart probe showed no evidence for rearrangement. (*E*) Coronal computed tomography scan of the chest ~6-mo postresection/amputation of the primary distal arm soft tissue mass demonstrating interval development of bilateral pulmonary metastases. (*F*) Hematoxylin and eosin (H&E) staining of the pretherapy forearm biopsy that shows a spindle cell neoplasm arranged in a fascicular pattern and characteristic of congenital fibrosarcoma. (*G*) Post-therapy H&E of resected lung metastases showed large areas of tumor necrosis. However, there remained persistent areas of viable tumor. Scale bar, 200 μm. (*H*) Tissue from the index case exhibits a high mitotic index with up to 50 mitoses per 10 high power fields. Yellow arrowheads indicate mitotic figures. Scale bar, 50 μm.

(Individualized Cancer Therapy [iCAT] Recommendation for Patients With Recurrent, Refractory or High Risk Solid Tumors; NCT01853345) (Janeway et al. 2014) and underwent full transcriptome sequencing in the Precision in Pediatric Sequencing (PIPseq) program at Columbia University Medical Center. Transcriptome analysis was performed on two tumor blocks, both of which consisted primarily of tumor with >60% lesional cells.

### *Cytogenetics*

Cytogenetic analysis identified a complex and hyperdiploid karyotype showing a balanced translocation between bands 2p21 and 15q24 resulting in a t(2;15)(p21;q24), an extra copy of der(15)t(2;15), gains of Chromosomes 2, 8, 15, 17, and 19 (Fig. 1C).

### *Array Comparative Genomic Hybridization*

Array comparative genomic hybridization (aCGH) showed clear copy-number transitions within *EML4* and *NTRK3*, with no copy-number alteration near the *ETV6* locus (Fig. 2B–D). The 5′ end of *EML4* and the 3′ end of *NTRK3* showed copy-number gain relative to the rest of Chromosome 2 and Chromosome 15, respectively, suggestive of a fusion between these genes and consistent with the karyotype. The additional copies of Chromosomes 8, 17, and 19 noted by karyotype were also clearly visible on array, while the remainder of the genome did not show significant changes (Fig. 2A).

### *RNA and Directed Sequencing*

Sequencing of RNA isolated from formalin-fixed paraffin-embedded tumor material was used to identify RNA sequences that spanned two disparate chromosomes and where the coding frame was predicted to be maintained in the fusion transcript. The highest scoring in-frame fusion was one spanning the *EML4* gene on Chromosome 2p and *NTRK3* on Chromosome 15q (Fig. 2E,F). The genomic coordinates of the RNA fusion junction localize to Chr2:42472827/Chr15:88576276. In addition, increased expression of *NTRK3* exons downstream from the fusion was seen on RNA expression data. Of note, *EML4* is transcribed from the Watson strand (+) while *NTRK3* transcribes from the Crick strand (–).

The read count track for *EML4* (Fig. 2E) and *NTRK3* (Fig. 2F) displays the count of strand-specific reads aligning to the respective genes. Read counts for opposing strands are negligible and are not displayed. As is common in RNA-seq data, there are reads aligning to introns, as well as exons, demonstrating what is likely to be nascent transcription of unspliced pre-mRNA. The exon RPKM (reads per kilobase per million mapped reads) track displays RPKM calculated over each exon and where the library size normalization factor was taken to be the number of reads aligning to exons only. The RPKM data exhibit robust expression of *NTRK3* exons downstream from the breakpoint compared with upstream. The splicing and fusion of exon 2 in *EML4* and exon 14 in *NTRK3* was detected by the FusionMap algorithm (Ge et al. 2011). As demonstrated in the *NTRK3* track (Fig. 2F), the actual genomic location of the fusion, and the beginning of transcription for *NTRK3*, appears to occur within intron 13 of *NTRK3*. There is no clear point after *EML4* exon 2 where transcription diminishes suggesting that a wild-type *EML4* is also being transcribed from the second copy of *EML4*.

No other pathogenic sequence variants were otherwise identified in our RNA-seq analysis.

## Functional Analyses

### *Verification of* EML4-NTRK3 *in Patient Sample*

Based on previously described gene fusion isoforms involving the *EML4* and *NTRK3* genes, oligonucleotide primers were designed to encompass previously known breakpoint junctions of *EML4-ALK* and *ETV6-NTRK3* (Knezevich et al. 1998b; Bourgeois et al. 2000; Wai et al. 2000; Soda et al. 2007; Choi et al. 2008; Shinmura et al. 2008; Heuckmann et al. 2012). Using primers complimentary to the sequence in exon 2 of *EML4* and exon 14 of *NTRK3*, reverse transcription followed by PCR (RT-PCR) from the patient's left-sided pulmonary lesions resulted in a product whose sequence verified the in-frame junction (Fig. 2G).

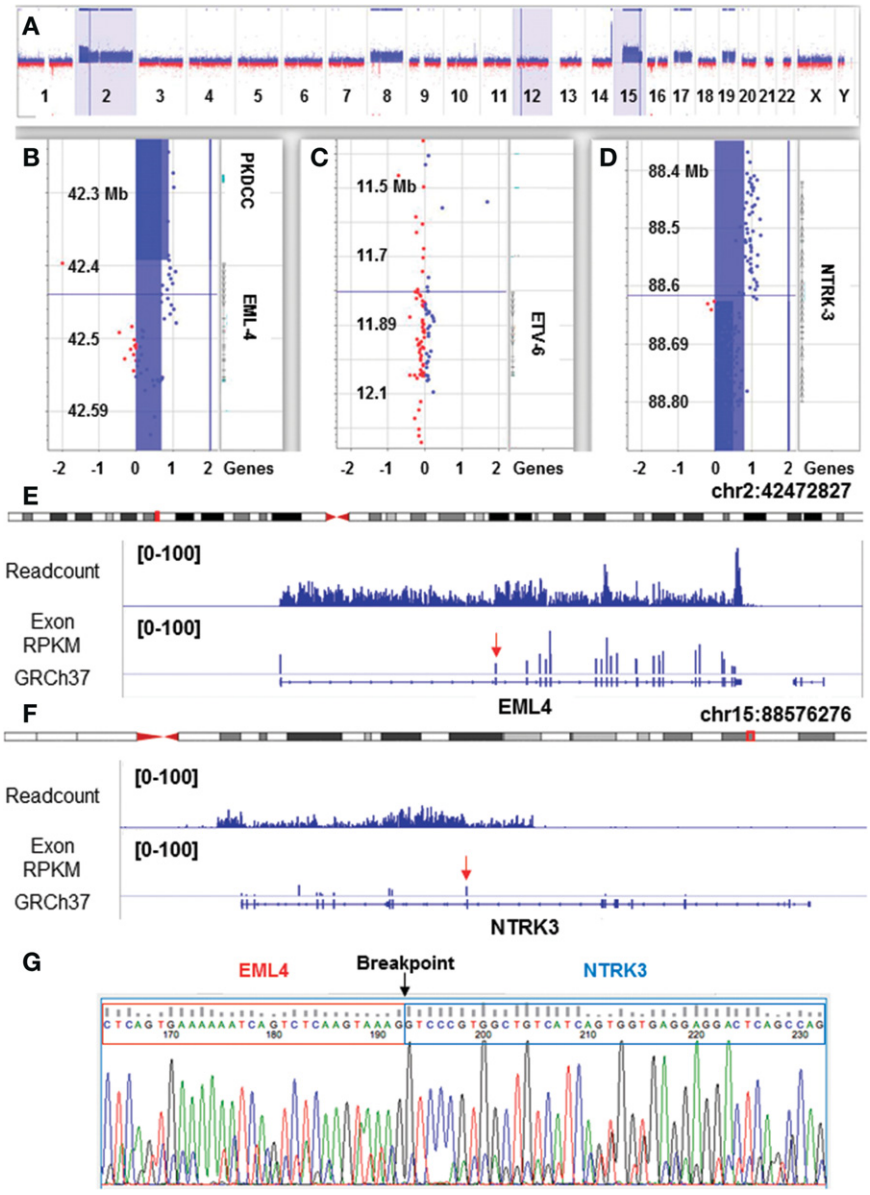


**Figure 2.** (*A–D*) Array comparative genomic hybridization (aCGH) showing copy-number gains at *EML4* and *NTRK3* with transitions at the breakpoints. Blue color represents copy-number gain and red color represents copy-number loss. (*A*) Overview of chromosomes with genes *EML4* (Chr2), *ETV6* (Chr12), and *NTRK3* (Chr15) highlighted. (*B*) *EML4* with a transition from high copy gain to low copy gain at intron 2. (*C*) No copy alteration at *ETV6*. (*D*) *NTRK3* with a transition from high copy gain to low copy gain at intron 12. (*E,F*) Transcriptional readout of the fusion between *EML4* and *NTRK3* from RNA-seq performed on primary tumor tissue. The GRCh37 track displays the Ensembl gene annotation using standard representations for exons, introns, and untranslated regions. *EML4* is transcribed from the Watson strand (*left* to *right*) while *NTRK3* transcribes from the Crick strand (*right* to *left*). RPKM data show robust expression of *NTRK3* exons downstream from the breakpoint in comparison to upstream. Red arrows indicate the two exons (exon 2 in *EML4* and exon 14 in *NTRK3*) whose splicing was detected using the FusionMap algorithm. The actual genomic location of the fusion localizes within intron 13 of *NTRK3*. No clear point after *EML4* exon 2 where transcription diminishes is observed suggesting that a wild-type *EML4* is also being transcribed from the second *EML4* gene copy. (*G*) Sanger sequencing confirmation of the in-frame fusion of *EML4* (exon 2) and *NTRK3* (exon 14).

### *Cloning and In Vitro Assessment of* EML4-NTRK3

We utilized a RT-PCR approach to cloning the entire coding sequence of the *EML4-NTRK3* fusion transcript using RNA isolated from primary pulmonary metastatic tissue. In silico analysis of the EML4-NTRK3 coding sequence (http://web.expasy.org/compute_pi/) predicts expression of a ~48 kDa protein. Examination of the NTRK3-encoding sequence reveals that the truncation of NTRK3 results in the loss of its transmembrane localization domain (http://atlasgeneticsoncology.org/ [Knezevich et al. 1998b]) and preservation of its protein kinase domain. In silico evaluation of the EML4 portion identifies an amino-terminal basic domain, a hydrophobic echinoderm microtubule-associated protein-like protein (HELP) domain and WD repeats (Choi et al. 2008). The truncation of the *EML4* portion in *EML4-NTRK3* results in preservation of exons 1–2 encoding only for part of the basic region which is encoded by exons 1–6 (Fig. 3A,B; Choi et al. 2008).

Murine fibroblast NIH 3T3 cells were transduced with packaged lentivirus encoding *EML4-NTRK3* (Fig. 3C). The expression of the fusion transcript was verified by RT-PCR with primers spanning the fusion breakpoint (Fig. 3D). The expression of protein was assessed by immunoblot using an *NTRK3*-directed antibody, demonstrating a protein at the predicted molecular weight (MW) of 48 kDa (Fig. 3E).

The ability of *EML4-NTRK3* to induce anchorage-independent growth was assessed by growth of cells in soft agar. Control NIH 3T3 cells transduced with empty vector yielded no colony formation, whereas cells transduced to express *EML4-NTRK3* resulted in macroscopic colony formation 21 d after inoculation of cells into soft agar suggesting the transformation of NIH 3T3 cells (Fig. 4A).

### *In Vivo Tumorigenicity*

To assess the in vivo effects of *EML4-NTRK3* expression, NIH 3T3 cells stably expressing *EML4-NTRK3* (NIH $3T3^{EML4\text{-}NTRK3}$) were injected subcutaneously into the flanks of immunodeficient mice. After 18 d of growth, mice injected with NIH $3T3^{EML4\text{-}NTRK3}$ cells had developed tumors that were nearly 2000 $mm^3$ in size necessitating euthanasia as per animal protocol guidelines. In contrast, mice injected with NIH 3T3 cells infected with empty vector showed no evidence of tumor formation (Fig. 4B). Furthermore, the histologic appearance of *EML4-NTRK3*-expressing tumors recapitulated the spindle cell herringbone pattern characteristic of congenital fibrosarcoma (Fig. 4C).

## DISCUSSION

We present a case of recurrent congenital fibrosarcoma that was responsive to multimodal therapy (chemoradiotherapy and surgery) despite the presence of extensive bilateral pulmonary metastases. The case did not harbor the characteristic *ETV6-NTRK3* fusion oncogene previously described in congenital fibrosarcoma, but was found to express a novel fusion gene involving *EML4* and *NTRK3*. Sequence verification and cloning of the *EML4-NTRK3* fusion gene allowed for functional characterization of this fusion protein. We show that expression of *EML4-NTRK3* in NIH 3T3 cells is sufficient for cellular transformation, similar to the *ETV6-NTRK3* fusion oncogene (Knezevich et al. 1998b).

*EML4* has also been described as a fusion partner with ALK to generate the *EML4-ALK* gene fusion, which has been shown to drive non-small-cell lung cancer carcinogenesis (Soda et al. 2007; Choi et al. 2008). The EML4-ALK fusion protein leads to constitutively activated tyrosine kinase activity (ALK) through autodimerization of the EML4 portion. There are at least 15 known transcripts of *EML4-ALK*, each with varying breakpoints within EML4 (Maus et al. 2012). In contrast to the variation in the breakpoints within *EML4*, truncation

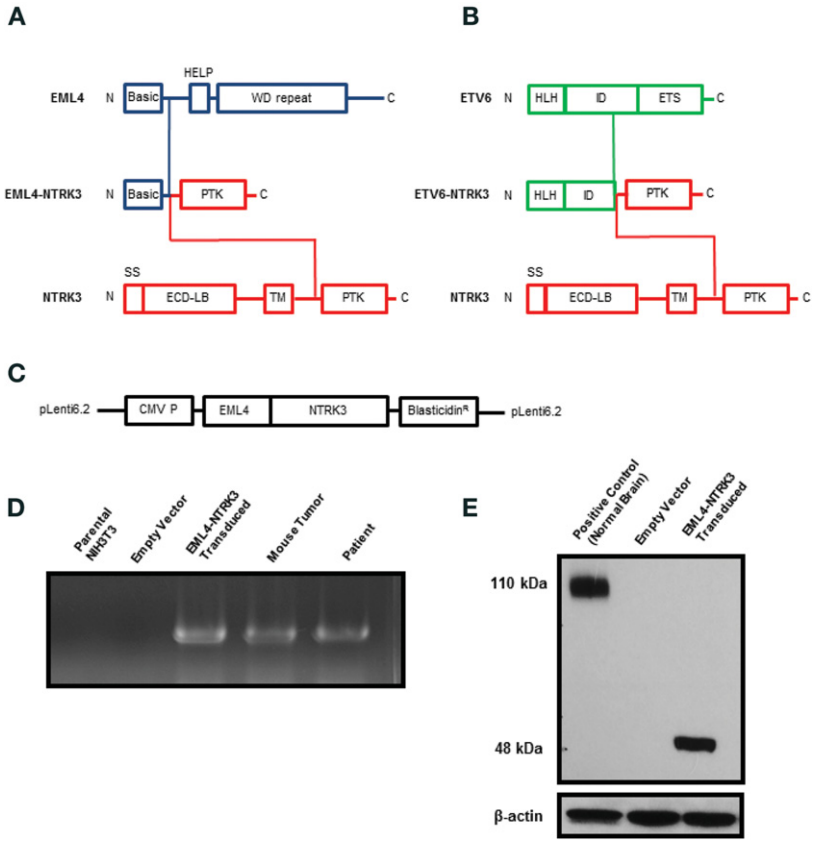


**Figure 3.** (*A*) (*Top*) Schematic of EML4 domains: Basic region, HELP domain, WD40 repeating domain; (*Middle*) EML4-NTRK3 predicted domains showing the contribution of the EML4 Basic region and the complete protein tyrosine kinase domain (PTK) of *NTRK3*. (*Bottom*) *NTRK3* domains: Signal peptide (SS), extracellular ligand binding domain (ECD-LB), transmembrane domain (TM), and protein kinase domain. (*B*) (*Top*) Schematic of ETV6 domains: Helix–loop–helix domain (HLH), internal domain (ID), ETS domain; (*middle*) ETV6-*NTRK3* predicted domains which fuses the HLH and ID regions of ETV6 to the entire PTK of NTRK3 similar to the EML4-NTRK3 fusion; (*bottom*) NTRK3 domains: signal peptide (SS), extracellular ligand binding domain (ECD-LB), transmembrane domain, and protein tyrosine kinase domain. (*C*) Schematic of lentiviral expression vector used for the stable transduction of *EML4-NTRK3*. (*D*) RT-PCR confirmation of the *EML4-NTRK3* fusion in stably transduced NIH 3T3 cells (NIH $3T3^{EML4\text{-}NTRK3}$), mouse tumors derived after subcutaneous injection of NIH $3T3^{EML4\text{-}NTRK3}$ cells, and tumor tissue derived from the patient's pulmonary metastasis. No *EML4-NTRK3* amplification was observed in either parental NIH 3T3 or empty vector NIH 3T3 cells which served as negative controls. (*E*) Immunoblot analysis confirming the expression of EML4-NTRK3 in stably transduced NIH $3T3^{EML4\text{-}NTRK3}$ cells using a monoclonal anti-NTRK3 antibody (EPR17341, Abcam). Brain lysate served as a positive control for the wild-type NTRK3 protein which migrates at ~110 kDa in comparison to the EML4-NTRK3 fusion protein (predicted MW 48 kDa). Protein lysate obtained from empty vector-transduced NIH 3T3 cells served as a negative control and shows no detectable band. β-Actin (Sigma-Aldrich) served as a loading control.

of the *ALK* gene is generally conserved resulting in the carboxy-terminal fusion of ALK from exon 20, and encompassing the entire protein kinase domain. Of note, *EML4-NTRK3* has also recently been identified in G111, a glioma cell line in an RNA sequencing initiative to identify oncogenic fusions in a large panel of cell lines (Klijn et al. 2015).

Analysis of the EML4-NTRK3 sequence reveals similarity in functional motifs to the previously described ETV6-NTRK3 that characterizes a significant proportion of congenital fibrosarcoma cases. The NTRK3 portion of EML4-NTRK3 maintains the entire kinase domain

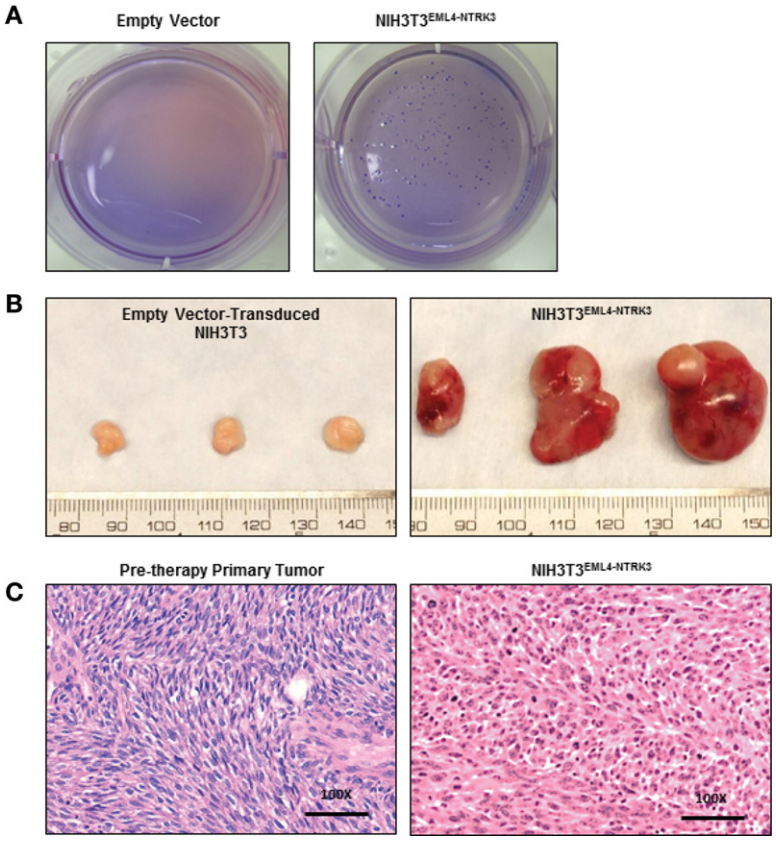


**Figure 4.** (*A*) Expression of *EML4-NTRK3* in NIH 3T3 cells promotes anchorage-independent growth. Empty vector (*left*) and *EML4-NTRK3*-expressing NIH 3T3 cells (NIH $3T3^{EML4\text{-}NTRK3}$, *right*) were grown in soft agar. Macroscopic colony formation was observed in NIH $3T3^{EML4\text{-}NTRK3}$ cells in contrast to empty vector control cells. Crystal violet staining was performed to visualize macroscopic colony formation. (*B*) Expression of *EML4-NTRK3* induces in vivo tumor formation in NOD *scid* γ (NSG) mice. Mice received subcutaneous flank injections of either empty vector-transduced NIH 3T3 cells or NIH $3T3^{EML4\text{-}NTRK3}$ cells (1 million cells/mouse). After 18 d following injection of cells, mice who received NIH $3T3^{EML4\text{-}NTRK3}$ cells (*right*) were euthanized in accordance with animal protocol guidelines which mandated euthanasia of animals harboring large tumors (>2000 $mm^3$). In contrast, mice injected with empty vector-transduced cells yielded only residual Matrigel plugs and no evidence of tumor (*left*). (*C*) Mouse tumors derived from NIH $3T3^{EML4\text{-}NTRK3}$ cells recapitulates the histology of congenital fibrosarcoma. The histology observed in the mouse tumor (*right*) demonstrates the characteristic herringbone pattern of spindle cells that was also seen in the primary patient tumor (*left*). Scale bar, 100 μm.

of NTRK3, and, just as in ETV6-NTRK3, lacks the transmembrane localization domain. ETV6-NTRK3 preserves the ETV6 contributing HLH domain resulting in HLH-mediated dimerization and ligand-independent activation of the NTRK3 kinase (Knezevich et al. 1998b; Bourgeois et al. 2000). In contrast, EML4-NTRK3 preserves only a small portion of the EML4 basic region and the protein kinase portion of NTRK3 in its entirety. It is therefore unclear at this time if EML4-NTRK3 activation behaves in a similar manner as ETV6-NTRK3.

The presence of hemimelia is a notable clinical feature described in this clinical case of congenital fibrosarcoma. Several signaling pathways involved in regulating limb bud patterning and outgrowth are also known to play key roles in oncogenesis including sonic hedgehog (SHH), fibroblast growth factor (FGF), and Wnt signaling pathways (Zuniga et al. 2012). For example, DKK1 has been shown to transform progenitor mesenchymal stem cells

into tumors resembling high grade sarcomas and has also been implicated in the development of congenital limb truncation anomalies in a mouse model constitutively expressing DKK1 under a mesodermal-specific promoter (Matushansky et al. 2007; Navarro et al. 2010; Gibault et al. 2011; Dela Cruz et al. 2012). However, it remains unclear whether segmental somatic mosaicism for the *EML4-NTRK3* fusion or other genes have contributed to the development of both the soft tissue tumor and hemimelia. Assessment of different normal tissues from the source patient for the *EML4-NTRK3* fusion may clarify this issue.

Identification of the novel *EML4-NTRK3* fusion in this recurrent case of congenital fibrosarcoma was enabled through clinical genomics efforts (e.g., PIPseq and iCAT) that are beginning to be incorporated in the diagnostic workup and molecular characterization of patients' cancers (Janeway et al. 2014). The identification of novel genes, as well as so-called "actionable mutations," through the sequencing of patient primary tumors will enable the rational matching of potentially effective agents that would not have otherwise been identified based on clinical features and presentation alone. To illustrate the potential clinical utility of sequencing tumors in the context of this clinical case, the identification of a novel *NTRK3*-containing fusion gene provides a preclinical rationale for the incorporation of crizotinib to the treatment regimen in the event of recurrent disease for this patient (Taipale et al. 2013).

Although cases of congenital fibrosarcoma carry an overall favorable prognosis, identification of older patients diagnosed with fibrosarcoma or patients with *ETV6-NTRK3*-negative disease, may represent a population of high-risk patients whose tumors are driven by novel genes such as *EML4-NTRK3*. It would be interesting to determine the prevalence of *EML4-NTRK3* in archival samples of *ETV6-NTRK3*-negative congenital fibrosarcoma and other fibrosarcomas and to correlate *EML4-NTRK3* status with clinical outcome. The positive response to cytotoxic chemotherapy as well as radiotherapy in this clinical case may be of clinical relevance to patients who are found to harbor the *EML4-NTRK3* fusion gene particularly adult fibrosarcoma cases which would otherwise be deemed to not be responsive to chemotherapy.

## METHODS

### Cytogenetic Analysis

G-band karyotype analysis was performed on metaphase preparations obtained from cells grown in short-term culture of fresh tumor tissue using standard methods. Karyotype was described according to the International System for Human Cytogenetic Nomenclature (International Standing Committee on Human Cytogenetic Nomenclature et al. 2009). FISH was performed on formalin-fixed paraffin-embedded tissue according to standard protocols using an *ETV6* break-apart probe (Abbott Molecular, USA). Fluorescence signals were captured after counterstaining with 4′,6-diamidino-2-phenylindole (DAPI) using the Cytovision Imaging system attached to a Nikon Eclipse 600 microscope (Applied Imaging).

### Array Comparative Genomic Hybridization

aCGH utilized Agilent SurePrint G3 CGH and SNP Cancer Microarray 4×180. Reference DNA was Agilent reference DNA. aCGH was performed in CLIA certified laboratories at Boston Children's Hospital and Claritas Genomics.

### RNA and Directed Sequencing

One paraffin block, each containing predominantly tumor, with at least 60% lesional tissue, was chosen from the excisional biopsy and resection specimens of the primary tumor. RNA was extracted using the Qiagen RNeasy Kit (Qiagen). Sequencing libraries were prepared

using the Illumina TruSeq Stranded Total RNA Library Prep Kit. Pooled, indexed libraries were sequenced on an Illumina HiSeq2000 (100 base, paired-end reads). Fifty-one million reads were obtained from the excision biopsy specimen and 110 million reads from the resection specimen. Following base-calling and alignment with the Tuxedo Suite, rejected reads were analyzed using FusionMap (Ge et al. 2011) with default parameters for RNA and alignment to GRCh37.3. The output was filtered to include in-frame fusions, with at least one rescued read and three unique seed reads, and exclude known, recurrent artifacts.

### Cloning of *EML4-NTRK3*

Total RNA was isolated from primary tissue obtained following resection of residual tumor using manufacturer's instructions (Qiagen). First strand cDNA was then generated also according to manufacturer's instructions (Life Technologies). In order to validate the presence of the *EML4-NTRK3* fusion, oligonucleotide primers localized to exon 2 of *EML4* and exon 14 of *NTRK3* were designed using Primer-BLAST (http://www.ncbi.nlm.nih.gov/tools/primer-blast) (*EML4* forward primer: AGA TCG CCT GTC AGC TCT TG, *NTRK3* reverse primer: ACT CTC TGT AGT GAA CTT CCG G). PCR cycling conditions were: 94°C for 2 min, followed by 32 cycles of 94°C for 30 sec, 55°C for 45 sec, 68°C for 1 min, and a final extension of 68°C for 7 min using Platinum Blue PCR SuperMix (Life Technologies).

After confirmation of the *EML4-NTRK3* fusion gene by RT-PCR, cloning primers were designed to amplify the complete coding sequence of the *EML4-NTRK3* gene fusion using the aforementioned PCR cycling conditions (*EML4* cloning forward primer: ATG GAC GGT TTC GCC G, *NTRK3* cloning reverse primer: CTA GCC AAG AAT GTC CAG GTA GA). The amplified *EML4-NTRK3* sequence was subcloned into a sequencing vector using the Topo-TA system according to manufacturer's recommendations (Life Technologies), and the coding sequence verified by Sanger sequencing (Genewiz). After confirmation of the *EML4-NTRK3* coding sequence, the fusion gene was subcloned into a plenti6.2/V5 lentiviral expression vector according to manufacturer's instructions (Life Technologies).

### Expression of *EML4-NTRK3*

After subcloning and sequence confirmation of *EML4-NTRK3* into the lentiviral expression vector, the expression vector was transfected into the 293TN packaging cell line according to manufacturer's instructions (Invitrogen packaging system). Lentiviral packaging using an empty vector control was also performed. Packaged virus was then harvested and used to infect NIH 3T3 cells (ATCC) using Polybrene (10 μg/mL, EMD Millipore). After two serial infections, cell culture medium was supplemented with blasticidin (5 μg/mL, Life Technologies) to select for blasticidin-resistant, EML4-NTRK3-expressing clones.

#### *Detection of EML4-NTRK3*

NIH 3T3 cells expressing EML4-NTRK3 (NIH 3T3$^{EML4\text{-}NTRK3}$), were harvested and the expression of EML4-NTRK3 was assessed by RT-PCR using breakpoint primers with the same PCR conditions as above. Cells analyzed were parental NIH 3T3 cells, empty vector-transduced NIH 3T3 cells, NIH 3T3$^{EML4\text{-}NTRK3}$, and primary tumor tissue obtained from in vivo mouse studies, and total RNA isolated from primary tumor derived from the case patient.

#### *Immunoblot Analysis*

Lysates of PBS-washed NIH 3T3 cells (both empty vector control and *EML4-NTRK3* transduced) were prepared using 500 μL lysis buffer (RIPA [Thermo Scientific]), protease inhibitor cocktail (Thermo Scientific), 10 mM $Na_4P_2O_7$, and 2 mM EDTA). The mixture was incubated

on ice for 30 min, vortexing every 10 min. It was then centrifuged at 13,200 rpm for 10 min, and the supernatant then collected and stored at −80°C. Using 4%–12% Bis–Tris Gels (Life Technologies), 5 μg of protein (mixed 1:1 with Laemmli buffer, Sigma-Aldrich) was analyzed and proteins subsequently transferred onto nitrocellulose iBlot Transfer Stacks (Thermo Scientific) using iBlot Gel Transfer Device. The membranes were incubated with 5% milk blocking solution for 45 min followed by an overnight incubation at 4°C using a carboxy terminus anti-TrkC antibody (1:500 dilution, EPR17341, Abcam). The membranes were subsequently washed with PBS-Tween 20 (0.5%) and incubated for 1 h with anti-rabbit IgG horseradish-peroxidase linked (1:5000 dilution, GE Healthcare UK) at room temperature. Membranes were again washed with PBS-Tween 20 (0.5%) and proteins were visualized with HyGlo Chemiluminescent solution (Denville Scientific).

### *Soft Agar Colony Formation Assay*

The soft agar assay for colony formation was performed according to an established protocol (Muller et al. 1993). Parental NIH 3T3 cells and NIH 3T3 cells stably transduced with *EML4-NTRK3*, cultured in DMEM F12 media (Life Technologies) with 10% FBS, 1% non-essential amino acids, and 1% penicillin/streptomycin, were plated in triplicate at a density of 5000 cells per well using a six-well plate format. The cells were suspended in soft agar (0.3% media/agarose/cell mixture). The plates were photographed 21 d after plating and stained with crystal violet (0.0025% crystal violet in 10% formalin buffer, Sigma-Aldrich).

### *Mouse Xenograft Modeling*

Three sets of 3 NOD-SCID γ null (NSG) mice (Jackson Laboratory) were used, all 8 wk old, and each set injected with either parental NIH 3T3 cells, empty vector NIH 3T3 cells, or *EML4-NTRK3* infected NIH 3T3 cells, respectively. One million cells were injected per mouse subcutaneously and tumor growth was measured weekly using calipers. Mice injected with *EML4-NTRK3* infected NIH 3T3 cells were euthanized as per animal protocol guidelines 18 d post injection due to the rapid formation and size of subcutaneous tumors (~2000 $mm^3$).

## ADDITIONAL INFORMATION

### Ethics Statement

Informed and signed consent was obtained and archived for the research performed and publication of the results. The patient was enrolled onto the multicenter targeted gene sequencing research study (Individualized Cancer Therapy [iCAT] Recommendation for Patients With Recurrent, Refractory or High Risk Solid Tumors; NCT01853345) with approval from the Columbia University Medical Center Institutional Review Board under protocol AAAJ5811. The patient was also consented for clinical sequencing at Columbia University Medical Center through the Precision in Pediatric Sequencing Program (PIPseq). Animal studies described in this manuscript have been approved by the Columbia University Medical Center Institutional Animal Care and Use Committee (IACUC) under protocol AAAF5850.

### Database Deposition and Access

Array comparative genomic hybridization data has been deposited in the Dryad Digital Repository (http://datadryad.org/) and registered under doi:10.5061/dryad.521j5, and RNA-seq data has been deposited in the NCBI Sequence Read Archive (SRA; http://www.ncbi.nlm.nih.gov/sra) under accession number SRP062247.

## Acknowledgments

F.S.D.C. would like to thank the St. Baldrick's Foundation for its continuing research support through the NetApp St. Baldrick's Scholar grant. F.S.D.C. would also like to thank and acknowledge research support by the Hyundai Hope on Wheels Hope Grant, the Jamie Deutsch Foundation, and the John M. Driscoll, Jr. Children's Fund grant.

## Author Contributions

S.T.-D., A.J.C., K.A.J., M.H.H., M.M.M., P.L.N., S.J.A., V.V.M., A.L.K., and F.S.D.C. designed the study and analyzed the data. S.T.-D., J.L.G.-B., A.J.C., K.A.J., M.H.H., M.M.M., P.L.N., V.V.M., A.K.-C., E.P.C., and F.S.D.C. collected clinical data. A.J.C, M.H.H., M.M.M., P.L.N., and V.V.M. reviewed pathology slides and collected pathology data. S.T.-D., S.J.A., A.L.K., F.S.D.C. performed the statistical analysis. S.T.-D., J.L.G.-B., A.J.C, M.H.H., M.M.M., V.V.M., A.L.K., and F.S.D.C. wrote and edited the manuscript. All authors edited the manuscript.

Competing Interest Statement

The authors have declared no competing interest.

Received July 1, 2015; accepted in revised form August 5, 2015.

## REFERENCES

Bourgeois JM, Knezevich SR, Mathers JA, Sorensen PH. 2000. Molecular detection of the ETV6-NTRK3 gene fusion differentiates congenital fibrosarcoma from other childhood spindle cell tumors. *Am J Surg Pathol* **24:** 937–946.

Choi YL, Takeuchi K, Soda M, Inamura K, Togashi Y, Hatano S, Enomoto M, Hamada T, Haruta H, Watanabe H, et al. 2008. Identification of novel isoforms of the EML4-ALK transforming gene in non-small cell lung cancer. *Cancer Res* **68:** 4971–4976.

Dela Cruz F, Terry M, Matushansky I. 2012. A transgenic, mesodermal specific, Dkk1 mouse model recapitulates a spectrum of human congenital limb reduction defects. *Differentiation* **83:** 220–230.

Ge H, Liu K, Juan T, Fang F, Newman M, Hoeck W. 2011. FusionMap: detecting fusion genes from next-generation sequencing data at base-pair resolution. *Bioinformatics* **27:** 1922–1928.

Gibault L, Perot G, Chibon F, Bonnin S, Lagarde P, Terrier P, Coindre JM, Aurias A. 2011. New insights in sarcoma oncogenesis: a comprehensive analysis of a large series of 160 soft tissue sarcomas with complex genomics. *J Pathol* **223:** 64–71.

Gupta A, Maddalozzo J, Win Htin T, Shah A, Chou PM. 2004. Spindle cell rhabdomyosarcoma of the tongue in an infant: a case report with emphasis on differential diagnosis of childhood spindle cell lesions. *Pathol Res Pract* **200:** 537–543.

Heuckmann JM, Balke-Want H, Malchers F, Peifer M, Sos ML, Koker M, Meder L, Lovly CM, Heukamp LC, Pao W, et al. 2012. Differential protein stability and ALK inhibitor sensitivity of EML4-ALK fusion variants. *Clin Cancer Res* **18:** 4682–4690.

International Standing Committee on Human Cytogenetic Nomenclature. Shaffer LG, Slovak ML, Campbell LJ. 2009. *ISCN 2009: an international system for human cytogenetic nomenclature (2009).* Karger, Basel, Unionville, CT.

Janeway KA, DuBois SG, Glade Bender JL, Kim A, Parker E, Church AJ, Crompton BD, Stegmaier K, Shusterman S, London WB, et al. 2014. Multicenter study assessing tumor molecular profiles in advanced pediatric solid tumors. *J Clin Oncol* **32:** 5s.

Klijn C, Durinck S, Stawiski EW, Haverty PM, Jiang Z, Liu H, Degenhardt J, Mayba O, Gnad F, Liu J, et al. 2015. A comprehensive transcriptional portrait of human cancer cell lines. *Nat Biotechnol* **33:** 306–312.

Knezevich SR, Garnett MJ, Pysher TJ, Beckwith JB, Grundy PE, Sorensen PH. 1998a. ETV6-NTRK3 gene fusions and trisomy 11 establish a histogenetic link between mesoblastic nephroma and congenital fibrosarcoma. *Cancer Res* **58:** 5046–5048.

Knezevich SR, McFadden DE, Tao W, Lim JF, Sorensen PH. 1998b. A novel ETV6-NTRK3 gene fusion in congenital fibrosarcoma. *Nat Genet* **18:** 184–187.

Matushansky I, Hernando E, Socci ND, Mills JE, Matos TA, Edgar MA, Singer S, Maki RG, Cordon-Cardo C. 2007. Derivation of sarcomas from mesenchymal stem cells via inactivation of the Wnt pathway. *J Clin Invest* **117:** 3248–3257.

Maus MK, Stephens C, Zeger G, Grimminger PP, Huang E. 2012. Identification of novel variant of EML4-ALK fusion gene in NSCLC: potential benefits of the RT-PCR method. *Int J Biomed Sci* **8:** 1–6.

Muller AJ, Pendergast AM, Parmar K, Havlik MH, Rosenberg N, Witte ON. 1993. En bloc substitution of the Src homology region 2 domain activates the transforming potential of the c-Abl protein tyrosine kinase. *Proc Natl Acad Sci* **90:** 3457–3461.

Navarro D, Agra N, Pestana A, Alonso J, Gonzalez-Sancho JM. 2010. The EWS/FLI1 oncogenic protein inhibits expression of the Wnt inhibitor DICKKOPF-1 gene and antagonizes β-catenin/TCF-mediated transcription. *Carcinogenesis* **31:** 394–401.

Orbach D, Rey A, Cecchetto G, Oberlin O, Casanova M, Thebaud E, Scopinaro M, Bisogno G, Carli M, Ferrari A. 2010. Infantile fibrosarcoma: management based on the European experience. *J Clin Oncol* **28:** 318–323.

Rubin BP, Chen CJ, Morgan TW, Xiao S, Grier HE, Kozakewich HP, Perez-Atayde AR, Fletcher JA. 1998. Congenital mesoblastic nephroma t(12;15) is associated with ETV6-NTRK3 gene fusion: cytogenetic and molecular relationship to congenital (infantile) fibrosarcoma. *Am J Pathol* **153:** 1451–1458.

Saylors RL III, Stewart CF, Zamboni WC, Wall DA, Bell B, Stine KC, Vietti TJ. 1998. Phase I study of topotecan in combination with cyclophosphamide in pediatric patients with malignant solid tumors: a Pediatric Oncology Group Study. *J Clin Oncol* **16:** 945–952.

Shinmura K, Kageyama S, Tao H, Bunai T, Suzuki M, Kamo T, Takamochi K, Suzuki K, Tanahashi M, Niwa H, et al. 2008. EML4-ALK fusion transcripts, but no NPM-, TPM3-, CLTC-, ATIC-, or TFG-ALK fusion transcripts, in non-small cell lung carcinomas. *Lung Cancer* **61:** 163–169.

Soda M, Choi YL, Enomoto M, Takada S, Yamashita Y, Ishikawa S, Fujiwara S, Watanabe H, Kurashina K, Hatanaka H, et al. 2007. Identification of the transforming EML4-ALK fusion gene in non-small-cell lung cancer. *Nature* **448:** 561–566.

Taipale M, Krykbaeva I, Whitesell L, Santagata S, Zhang J, Liu Q, Gray NS, Lindquist S. 2013. Chaperones as thermodynamic sensors of drug-target interactions reveal kinase inhibitor specificities in living cells. *Nat Biotechnol* **31:** 630–637.

Tognon C, Knezevich SR, Huntsman D, Roskelley CD, Melnyk N, Mathers JA, Becker L, Carneiro F, MacPherson N, Horsman D, et al. 2002. Expression of the ETV6-NTRK3 gene fusion as a primary event in human secretory breast carcinoma. *Cancer Cell* **2:** 367–376.

Wai DH, Knezevich SR, Lucas T, Jansen B, Kay RJ, Sorensen PH. 2000. The ETV6-NTRK3 gene fusion encodes a chimeric protein tyrosine kinase that transforms NIH3T3 cells. *Oncogene* **19:** 906–915.

Zuniga A, Zeller R, Probst S. 2012. The molecular basis of human congenital limb malformations. *Dev Biol* **1:** 803–822.